Springtime Soil Moisture Teleconnections Drive Summertime Warming in the Western United States

Lily N. Zhang,[a] David S. Battisti,[a] Lucas R. Vargas Zeppetello,[b] Marysa M. Laguë[c]

[a] *Department of Atmospheric and Climate Science, University of Washington, Seattle, WA*

[b] *Department of Environmental Science, Policy, and Management, University of California, Berkeley, Berkeley, CA*

[c] *Department of Geography, University of British Columbia, Vancouver, BC, Canada*

Corresponding author: Lily N. Zhang, lnzhang@uw.edu

ABSTRACT

A prior study observed that regional variations in springtime soil moisture over the American Southwest are associated with distal summertime temperature and precipitation anomalies across the Western United States. Here, we perform an ensemble of soil moisture depletion experiments within the Community Earth System Model (CESM2) and show that a reduction in March surface soil moisture over the Southwest US causes positive May-June temperature anomalies throughout the Western US and precipitation anomalies in the Northwest that are consistent with observations. In our experiments, daytime diabatic heating over anomalously dry land surfaces in early spring excites circulation anomalies that evolve into a hemispheric-scale pattern similar to that observed following anomalously dry springtime in the Southwest US. We show that the subsequent late spring and early summer circulation anomalies are associated with large-scale reductions in atmospheric moisture and cloudiness that contribute to the near-surface warming. Our results suggest that land-atmosphere coupling provides a pathway for soil moisture variations to become a source of predictability on seasonal time scales in the Western US.

SIGNIFICANCE STATEMENT

Observations show that warmer-than-average summertime temperatures in the Western US are often preceded by drier-than-average spring soils in the Southwest US. We perform experiments within a global climate model and demonstrate the causal mechanism for this phenomenon: early spring soil moisture deficits in the Southwest US cause anomalously warm summers throughout the Western US through their effect on the large-scale atmospheric circulation.

1. Introduction

Temporally lagged correlations between climate state variables are an important indicator of predictability in the climate system. When these relationships extend across large spatial scales, they give rise to so-called “teleconnections” that are typically associated with prominent models of climate variability (Ångström 1935). Most notably, variations in sea surface temperature (SST) associated with the El Niño Southern Oscillation (ENSO) are known to influence precipitation at distal locations through atmospheric teleconnection pathways between the tropical Central Pacific and other parts of the world (Walker and Bliss 1932; Ropelewski and Halpert 1987; Trenberth et al. 1998). Less well-studied are the

teleconnection-like behaviors observed in other slow-varying components of the coupled climate system, such as land and sea ice (Teng et al. 2019; Xue et al. 2022; Liu et al. 2023).

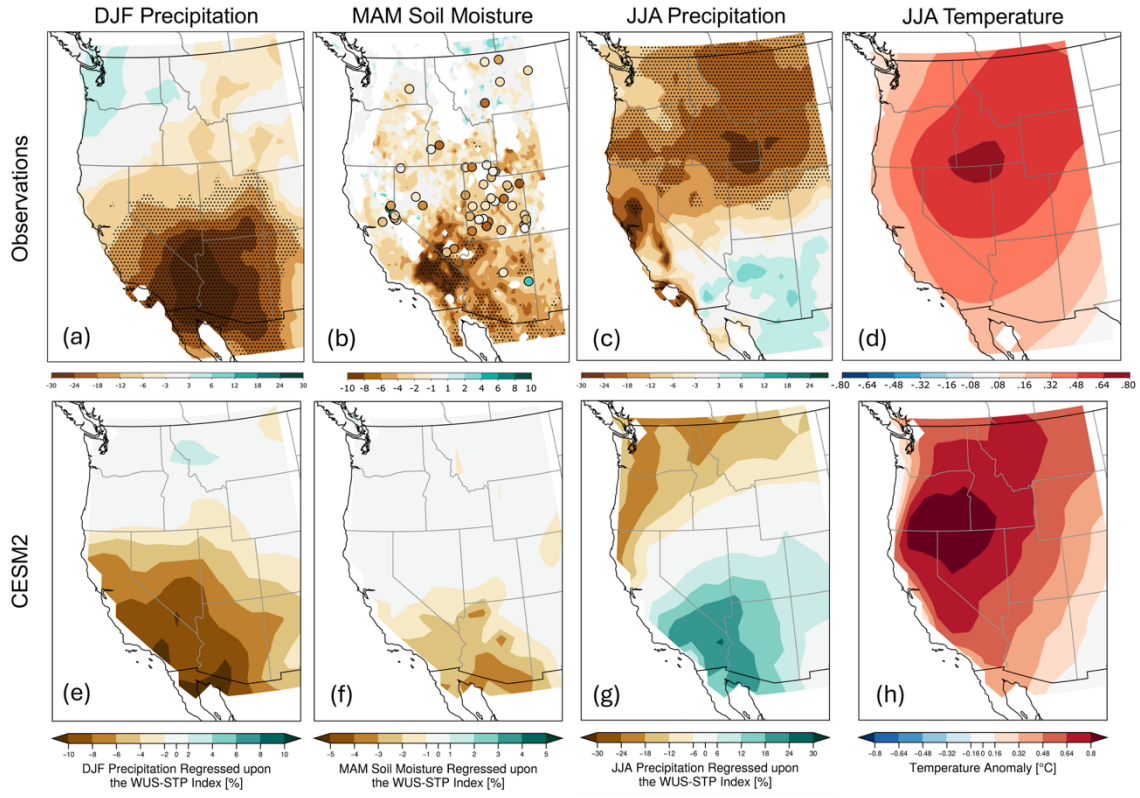

Fig. 1. EOF1 of high pass-filtered JJA average temperatures across the Western US domain (last panel) regressed against (a) DJF precipitation (b) MAM soil moisture and (c) JJA precipitation anomalies in observations (top) and the CESM2 historical simulation (e-h). The WUS-STP index captures 54% of interannual variability in Western US summertime temperatures (shown in parenthesis). Variations in soil moisture and precipitation are expressed as percentages relative to the climatological seasonal mean. Figure reproduced from Vargas Zeppetello et al. (2024). See methods for a description of data sources.

A recent study by Vargas Zeppetello et al. (2024) found that interannual summertime temperature variations associated with the leading pattern of Western US summertime temperature variability are anticorrelated with antecedent springtime soil moisture variations. Across CMIP models and in observations, springtime soil moisture deficits in the Southwest US are linked to summertime precipitation deficits and anomalously high temperature across much of the Western US (Fig. 1). Unlike most patterns of climate variability, the Western US summertime temperature pattern (WUS-STP) displays no statistical relationship with SST variability in summer nor in the preceding seasons—suggesting that distal soil moisture anomalies influence climate in subsequent seasons in a teleconnection-like manner through land-atmosphere interactions alone.

Soil moisture anomalies modulate the partitioning of surface latent and sensible heat fluxes and thus act as a local diabatic heating source over dry surfaces (Seneviratne et al.

2010). Locally, feedbacks between soil moisture, near-surface temperature, and precipitation have been shown to contribute to the persistence of extreme events such as heatwaves and drought (Schär et al. 1999; Lorenz et al. 2010; Zhou et al. 2019; Vargas Zeppetello et al. 2022). The time scales of these local interactions can extend over several months in some regions, making soil moisture a valuable source of seasonal predictability (Delworth and Manabe 1989; Fennessy and Shukla 1999; Dirmeyer 2000; Wu and Dickinson 2004; Koster et al. 2010, 2011; Guo et al. 2011; Paolino et al. 2012; Rahman et al. 2015). Of particular relevance to our study is the work by Fischer et al. (2007) who used a regional climate model forced by real-world lateral boundary conditions to investigate the role of soil moisture-atmosphere interactions during the 2003 European summer heat wave. Their sensitivity experiments showed that preceding spring soil moisture deficits in France amplified the summertime temperature anomalies through their effect on the local surface energy budget. There is strong evidence to suggest that the contiguous United States (CONUS) is another such region where soil moisture variations can exhibit strong "memory" characteristics on seasonal time scales (Liu et al. 2014; McColl et al. 2017; Rahmati et al. 2024). Rind (1982) used an atmosphere general circulation (AGCM) to demonstrate that reducing late spring soil moisture within the interior of the United States led to significantly higher near-surface temperature throughout CONUS during the summer. Following the North American summer drought of 1988, Namias (1991) hypothesized that antecedent soil moisture variations in early spring were a key indicator of anomalously low rainfall in early summer. A later study by Pal and Eltahir (2010) similarly concluded that feedbacks between antecedent soil moisture conditions and convective rainfall played a significant role in maintaining the persistence of the 1988 drought in a series of regional model experiments. More generally, Wu (2006) examined co-variability between spring soil moisture and summer precipitation and found statistically significant correlations over CONUS in a 50-year AGCM simulation. These early modeling studies all point to a link between spring soil moisture variations and summertime climate over the United States that is consistent with observations of the Western US summertime temperature pattern (Vargas Zeppetello et al. 2024).

Although the ability for antecedent soil moisture variations to influence climate beyond a single season has been established in models and observations, the spatial scales of these interactions are not as well understood. A few studies have explored the possibility for soil moisture anomalies to have non-local impacts through feedbacks that modify the atmospheric circulation, particularly in monsoonal regions (Shukla and Mintz 1982; Small 2001; Douville

2002; Rai et al. 2015; Berg et al. 2017; Ullah et al. 2021). A recent study by Teng et al. (2019) demonstrated that prescribing soil moisture deficits over select CONUS domains led to circumglobal circulation changes that produced a robust, non-local climate response. In their AGCM experiments, diabatic heating anomalies generated by a deficit in summertime soil moisture excited stationary wave anomalies that resembled waveguide teleconnection patterns (Branstator 1990, 2002). On average, these non-local effects manifest as a hemispheric scale stationary wave train the midlatitudes, including an anomalous high over the Pacific Northwest that matches the stationary wave response in similar experiments performed by Koster et al. (2016). With the aid of a stationary wave model, Koster et al. (2016) further confirmed that the diabatic heating anomalies obtained from prescribing rainfall deficits over CONUS land surfaces explained the stationary wave response in the AGCM. It is notable that the contemporaneous temperature anomalies associated with the summertime wave train identified by Koster et al. (2016) and Teng et al. (2019) resemble the pattern of summertime temperature variability and associated fluctuations in geopotential height observed by Vargas Zeppetello et al. (2024).

In this study, we perform an ensemble of soil moisture depletion experiments to understand the physical processes behind the Vargas Zeppetello et al. (2024) finding that springtime soil moisture anomalies in the Southwest US cause non-local summertime temperature and precipitation anomalies throughout the Western US via soil moisture induced atmospheric teleconnections.

2. Methods

a. CESM2 soil moisture depletion experiments

We utilize the Community Earth System Model (CESM2; Danabasoglu et al. 2020) in an atmosphere/land-only configuration with prescribed phenology and pre-industrial forcings. The land and atmospheric components of CESM2 are the Community Land Model Version 5 (CLM5; Lawrence et al. 2019) and the Community Atmosphere Model Version 6 (CAM6), respectively. In place of a coupled ocean model, the CAM6 atmosphere in our experiments is forced by prescribed monthly mean SST sea ice climatologies taken from the fully coupled CESM2 pre-industrial (PI) control run; simulations use PI (1850) CO2 levels of 285 ppm. We run this configuration, hereafter referred to as "CAM6-PI," at 0.9º x 1.25º resolution to obtain monthly output of relevant climate variables.

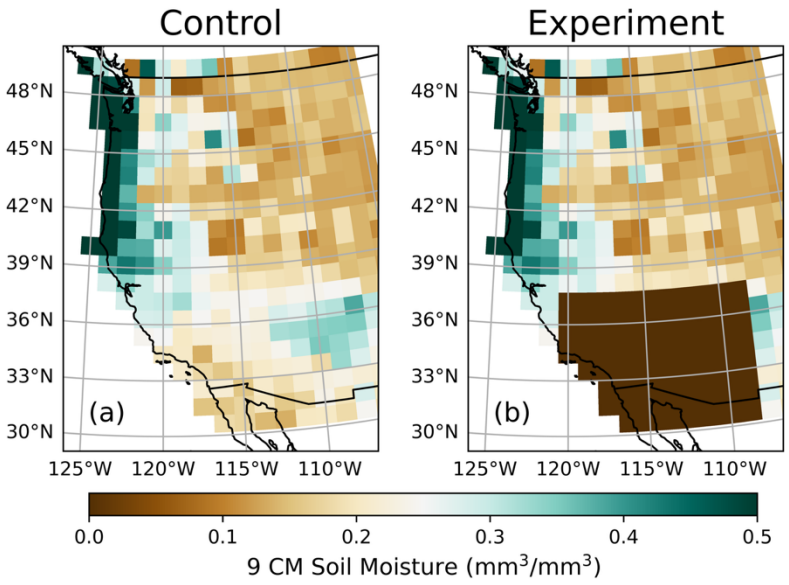

Fig. 2. Depth-weighted volumetric soil moisture content of the top three model layers (~9 cm) in the CLM restart files for March 1 of (left) an example control run year and (right) a Southwest US depletion experiment run in the same year.

Using CAM6-PI as a starting point, we instantaneously deplete soil moisture over a specified domain by modifying the soil liquid water field within the CLM restart files. In our Southwest US experiments, we set the soil liquid water content of the top three model layers (~9 cm) to zero on March 1st of each simulation year for land units between 108-120ºW and 30-38ºN (Fig. 2). We chose to only modify the initialization of the land surface, rather than prescribe soil moisture deficit over a longer period as Koster et al. (2016) and Teng et al. (2019) did, to represent the observed effects of anomalously low wintertime precipitation on spring soil moisture in the Southwest US (Fig. 1a). When directly compared to a control run advanced with the same restart files (i.e., all else being equal), our experiment isolates the impact of anomalously dry land surfaces in the Southwest US on global climate over the timescales we are interested in—from the start of spring until summer.

To remove the influence of internal variability on our results, we examine an ensemble of soil moisture depletion experiments, each with a unique initial state. We create the ensemble by duplicating the restart files from a 108-year CAM6-PI control run. Then, in each March 1st restart file, we deplete the soil moisture in the Southwest domain (as above) and run the model for six months to the end of August, resulting in 108 soil depletion experiments. Each year of the YYY year experiment is initialized with the corresponding CAM6-PI year's restart file, such that there should be no signal of the current experiment year in the subsequent experiment year. All the results we present show evolution of the differences

between the control run and experiment, averaged across all 108 simulations, to yield the ensemble average response to the soil moisture depletion under a variety of initial conditions.

b. Observational data sources

To compare the results of our modeling experiment with observation-based data, we obtain monthly mean 2-m temperature and 500 mb geopotential height from ERA5 (Hersbach et al., 2023). We analyze these atmospheric variables alongside monthly averaged soil moisture values from 2001-2020, which are computed from daily satellite measurements from version 7 of the European Space Agency's Climate Change Initiative (CCI; Dorigo et al. 2017).

Figure 1, which was reproduced from Vargas Zeppetello et al. (2024), uses ESA CCI soil moisture over the same period (2001-2020), in-situ soil moisture from the International Soil Moisture Network (ISMN; Dorigo et al., 2011), station-based precipitation data from CRU TS (1981-2020; Harris et al., 2020), and temperature reconstructions from Berkeley Earth (1850-2021; Rohde et al., 2013).

3. Near-surface temperature response

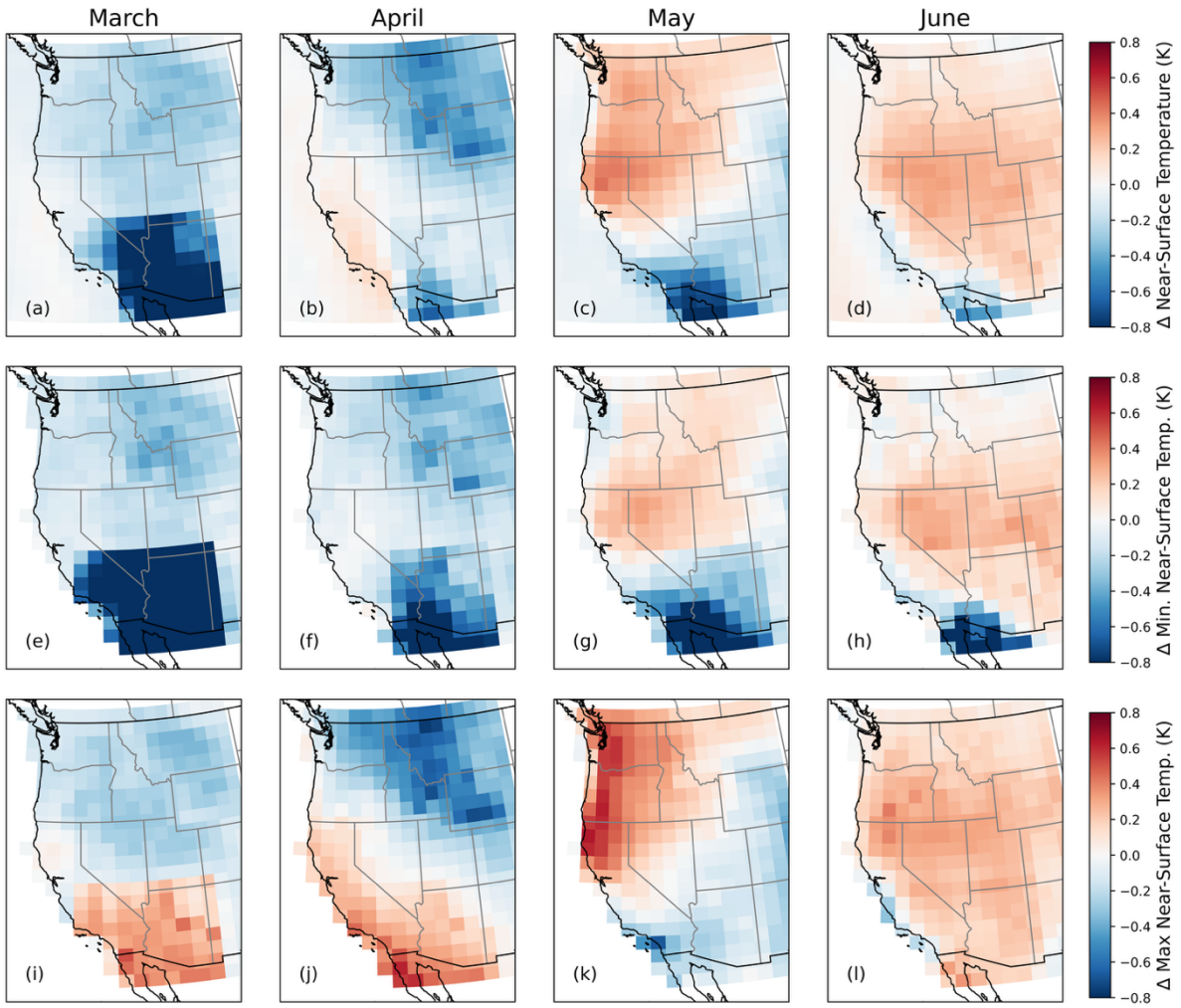

Fig. 3. March-June changes in (top) average (center) minimum and (bottom) maximum daily 2-m temperature as a result of March Southwest US soil moisture depletion, averaged across 108 ensemble members.

As a result of depleting surface soil moisture over the Southwest US at the start of March, we find warming in the Western US (WUS) across the average, minimum, and maximum daily near-surface temperature fields in May-June (right two columns in Fig. 3). The daily average temperature anomalies in May are roughly +0.3ºC over the Pacific Northwest while the daytime maximum temperature anomaly is as high as +0.6ºC over some grid cells. By June, warming becomes more widespread, extending over most of the WUS region and with an average temperature anomaly of +0.2ºC. The spatial pattern of warming in our experiments is consistent with observations of the WUS-STP, which also manifests most prominently over Southern Idaho and surrounding regions (cf. Fig. 1d with 3d). However,

unlike the WUS-STP, the warm anomalies fade in July and are entirely absent later in the summer (not shown).

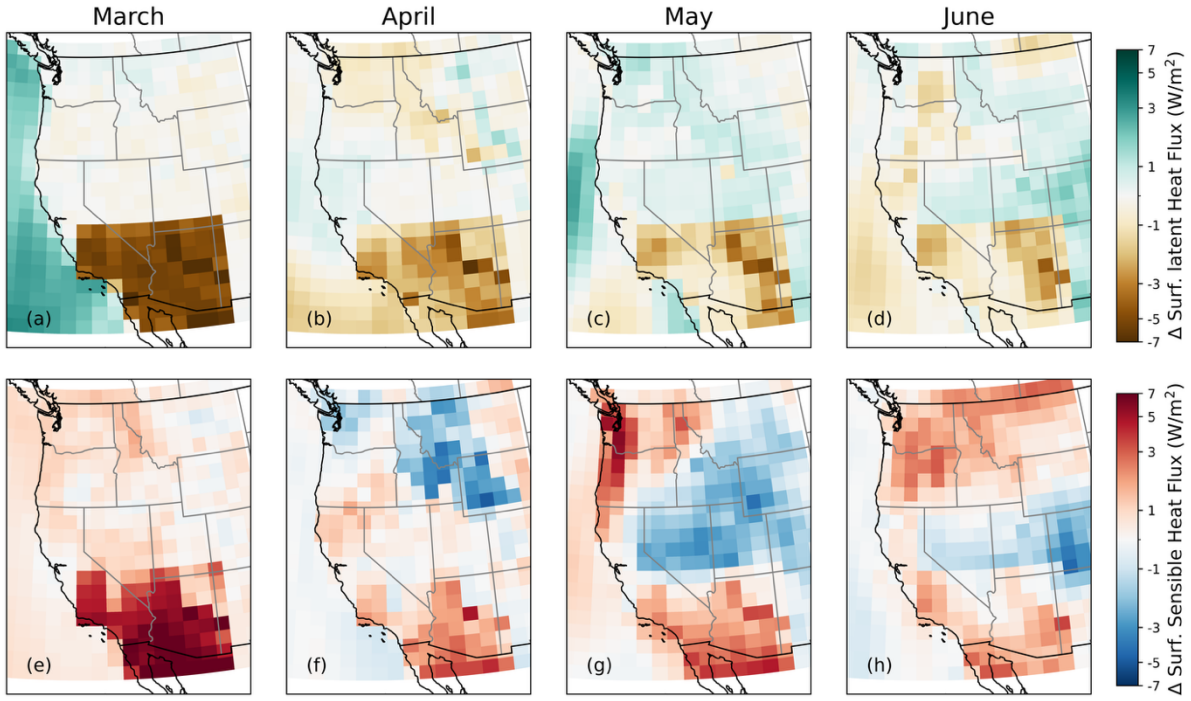

Fig. 4. March-June changes in surface (top) latent and (bottom) sensible heat flux as a result of March Southwest US soil moisture depletion, averaged across 108 ensemble members.

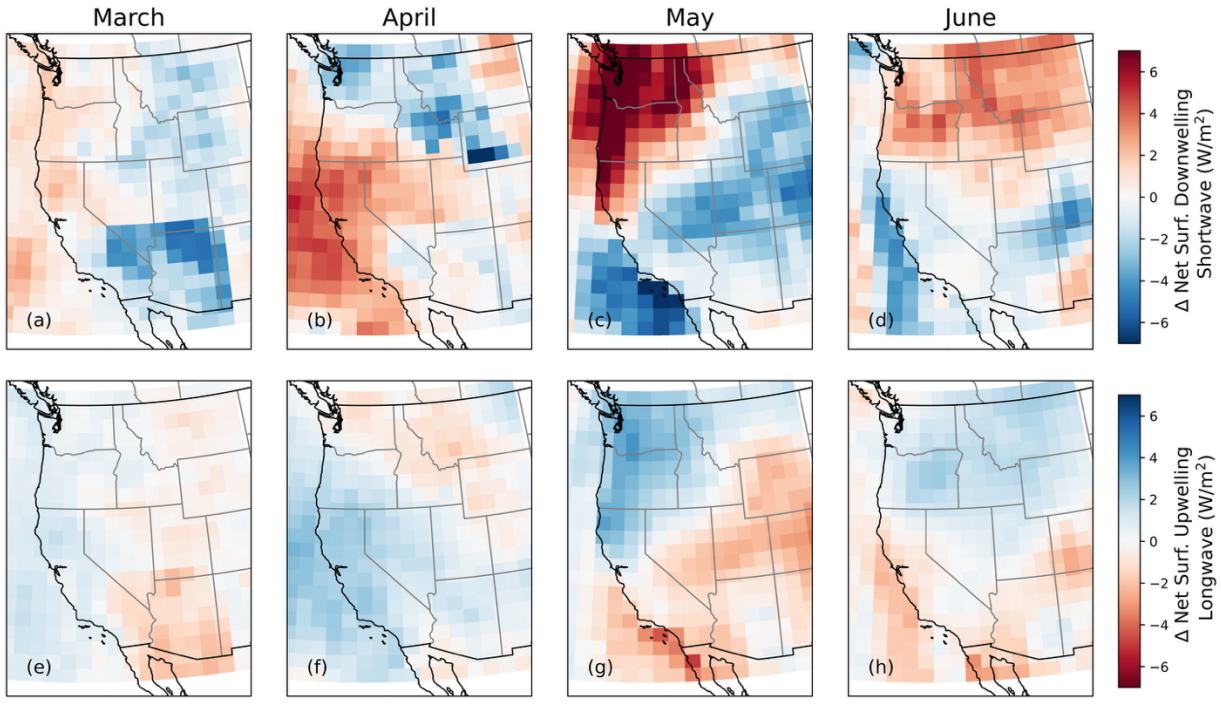

Fig. 5. As in Fig. 4, but for changes in net surface (top) downwelling shortwave and (bottom) outgoing longwave radiation.

To explain the May-June temperature response, we analyze the relevant components of the surface energy budget (Figs. 4 and 5). Although early summer warming appears to coincide with increases in upward surface sensible heat flux over the Northwest US, there is no accompanying decrease in upward latent heat flux that would link warming to changes in evaporative fraction (Fig. 4). Instead, we find a pronounced increase in net downwelling surface shortwave over the northern portion of our domain, particularly in May, that is spatially coincident with the temperature response (Fig. 5); this increase in solar heating is accompanied by a slightly weaker increase in surface upwelling longwave radiation that is likely driven by the surface temperature change. Over the southeast portion of our domain, we find the opposite to be true: solar heating and surface longwave emission both decrease at the surface, which is consistent with the slight cooling in May (Fig. 3). The surface sensible heat flux also appears to decrease directly southeast of the warming, but this signature is interrupted by the lingering bounds of the soil moisture depletion patch imposed over the Southwest US (Fig. 4g).

Surprisingly, the daily average temperature decreases in March over the Southwest US by more than 0.8ºC where soil moisture was depleted (Fig. 3), despite sharp Bowen ratio changes in Figure 4 that would suggest the opposite (warming). We reconcile this finding by noting that the adiabatic cooling at night that is associated with the large-scale response in the second half of the month is greater than the daytime diabatic heating associated with the shift in the Bowen ratio due to soil moisture depletion (see Sect. 5).

4. Propagation of large-scale moisture anomalies

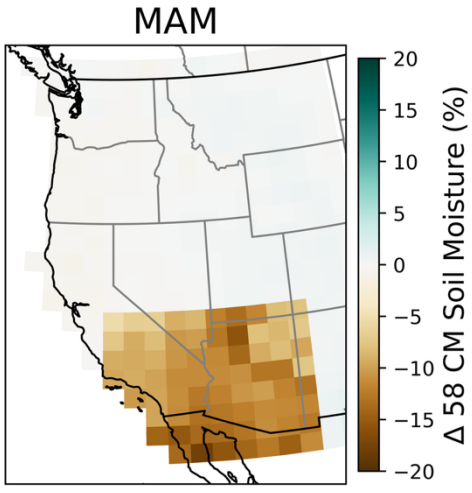

Fig. 6. Changes in March-May (MAM) averaged top 58 CM soil moisture as a result of March Southwest soil moisture depletion, averaged across 108 ensemble members. Anomalies are computed as a percentage relative to seasonal mean climatologies obtained from the control run.

Figure 6 shows the reduction in springtime [March-May (MAM)] averaged top 58 cm soil moisture produced by our experiment. Despite only prescribing a one-time, near-surface deficit on the first of March, we find negative soil moisture anomalies in the Southwest US that persist throughout the top half meter of soil and affect the seasonal mean for the region—this is consistent with in-situ observations analyzed in Vargas Zeppetello et al. (2024) that showed consistent variations between surface soil moisture and seasonal means at depth up to 50 cm. Averaged over MAM, our March 1st depletion experiments reduce 58 cm soil moisture an average of 10% relative to the MAM climatological mean; compared to the region's typical year-to-year variations in MAM soil moisture in the model, this represents a 1.2σ anomaly.

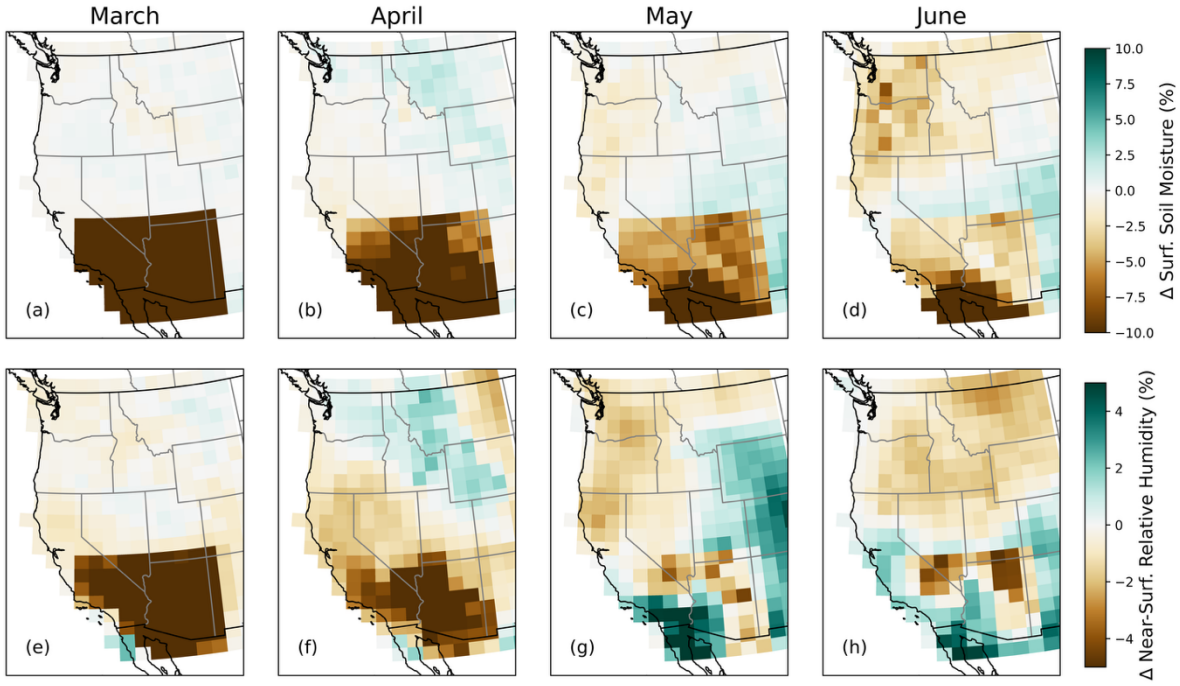

Fig. 7. March-June changes in (top) 10 CM soil moisture and (bottom) 2-m relative humidity as a result of March Southwest soil moisture depletion, averaged across 108 ensemble members. Both anomalies are computed as a percentage relative to monthly mean climatologies obtained from the control run.

Figure 7 reveals the month-to-month evolution of surface soil moisture and low-level relative humidity anomalies in our experiments. Although we initially set soil moisture to zero at the start of March, soil moisture gradually increases over the Southwest US due to precipitation and snow melt (Fig. 7a-d). Across the six months of our experiment, the anomalies in surface soil moisture and low-level relative humidity appear to be correlated

with one another (Fig. 7). From March to June, the surface soil moisture deficits initially have a strong impact on the overlying atmosphere and induce negative changes in low-level relative humidity over the Southwest that then appear to propagate northward to the Pacific Northwest by May. Unlike the temperature anomalies in our experiment, this pattern of soil moisture deficit persists well into July and August (not shown).

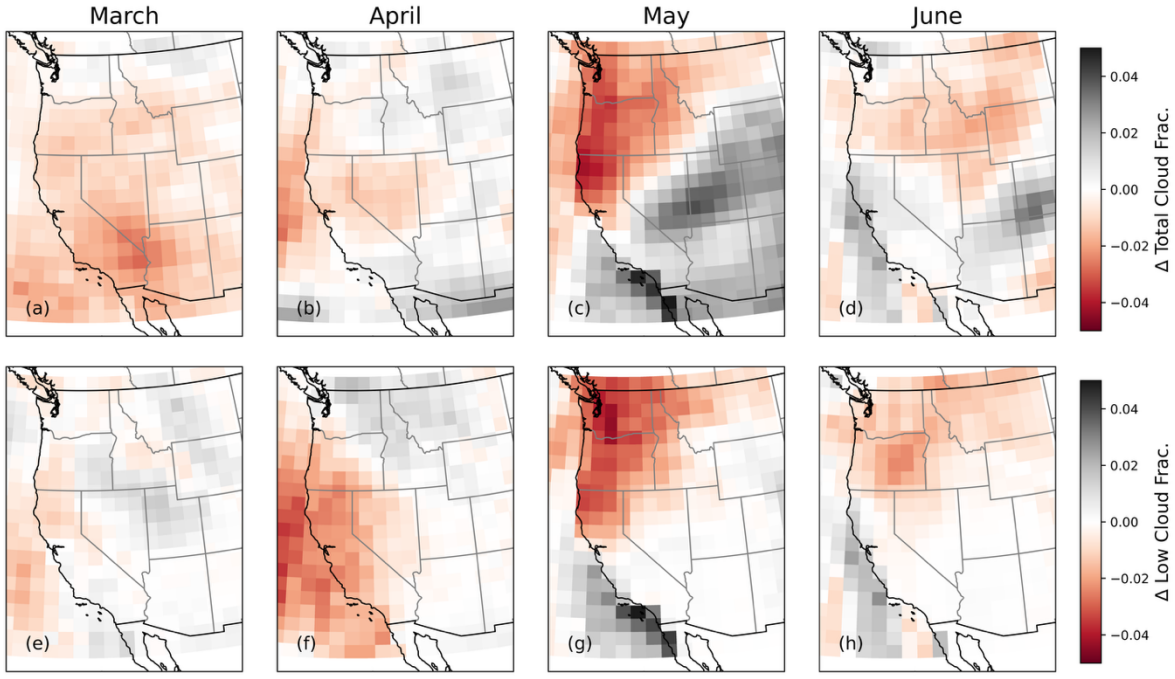

Fig. 8. Changes in (top) total cloud and (bottom) low cloud fraction as a result of March Southwest US soil moisture depletion, averaged across 108 ensemble members.

To understand the aforementioned changes in surface shortwave radiation that drive the May-June warming in our experiments, we note that decreases in low-level relative humidity (Figs. 7e-h) are accompanied by changes in cloudiness, particularly in the low cloud fraction (Figs. 8c,d,g,h). The albedo of low clouds is the primary contributor to the shortwave cloud radiative effect (SWCRE), and the decreases in low cloud fraction in May-June align with the areas of increased net downwelling shortwave in Figure 5c,d. These results confirm that changes in atmospheric moisture and cloudiness, not evaporative fraction, are what drive May-June warming in our experiment.

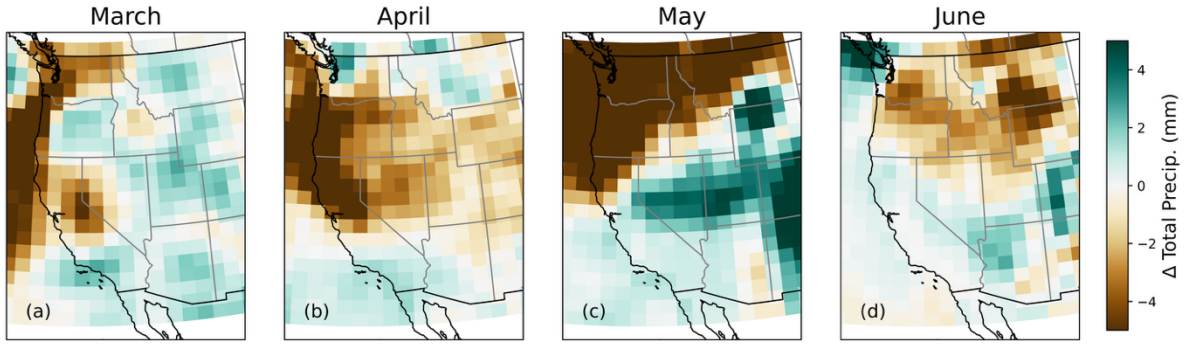

Fig. 9. Changes in total monthly precipitation as a result of March Southwest US soil moisture depletion, averaged across 108 ensemble members.

Total precipitation in the Northwest US also decreases in the experiment during April-June where there are coincident large-scale deficits in low-level relative humidity and cloudiness (Fig. 9). The resulting pattern of precipitation anomalies in the northern domain in May-June is similar to the observed precipitation anomalies in summertime associated with springtime soil moisture deficits (cf. Fig. 9c, d with Fig. 1c).

The propagation of large-scale moisture anomalies from the Southwest US to Pacific Northwest from March to early summer in our experiments is strong evidence of teleconnection-like behavior which must be initiated by soil moisture variations, which begs the question: What drives changes in atmospheric circulation to provide a pathway for these soil moisture teleconnections?

5. Circumglobal circulation changes

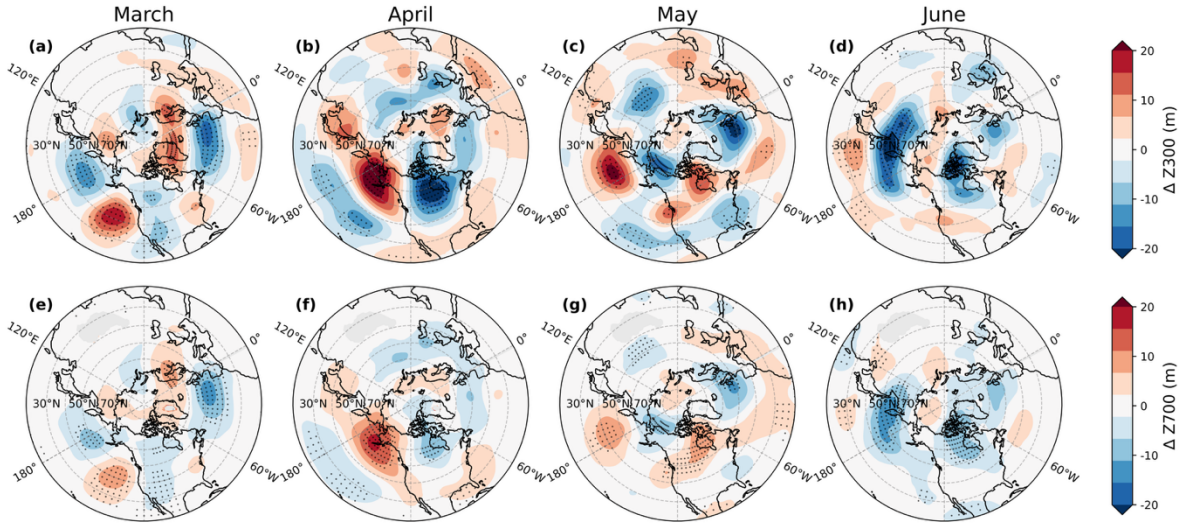

Fig. 10. March-June changes in (top) 300 and (bottom) 700 hPa geopotential heights as a result of March Southwest US soil moisture depletion, averaged across 108 ensemble members. Stippling indicates where the anomalies are significant at the 90% confidence level, based on a paired t-test.

To understand the large-scale response and connect March surface soil moisture deficit to subsequent changes in atmospheric moisture that appear in the Western US in April-June, we follow Koster et al. (2016) and Teng et al. (2019) and document the atmospheric circulation response to the soil moisture depletion. During spring, we find circumglobal changes that are vertically coherent throughout the troposphere (Fig. 10). Geopotential height anomalies in March and May form a nearly zonal pattern of alternating highs and lows in the midlatitudes that resembles a Rossby wave train. In March, a quasi-stationary high appears just off the West Coast of the US that deepens and extends north to form a meridional dipole in April. In May, a high-pressure anomaly over the Pacific Northwest coincides with large-scale warming and deficits in humidity, precipitation, and cloud fraction (Figs. 7g, 9c, and 7c), which persists into June but only aloft (Fig. 10d). The pattern of circulation anomalies in May-June (and the associated temperature and precipitation anomalies in Figs. 3cd, 9cd) strongly resemble the circulation responses to summertime moisture deficits previously demonstrated by Koster et al. (2016) and Teng et al. (2019) as well as observations of the summertime circulation anomalies associated with the WUS-STP (Vargas Zeppetello et al. 2024). As in their studies, the large-scale changes in moisture that drive near-surface drying and warming in May-June of our experiments can be explained by increased subsidence associated with the upper-level positive height anomaly over the Northwest US. Earlier reductions in precipitation and cloudiness during April likely result from the blocking effect of the east-west dipole in height anomalies flanking the west coast of Canada and the reduction in the westerlies farther offshore along 45ºN, which acts to disrupt the supply of moisture from the Pacific to the California coast. From June onwards, the positive geopotential height anomalies weaken considerably and dissipate, along with the positive temperature anomalies, in late summer (not shown).

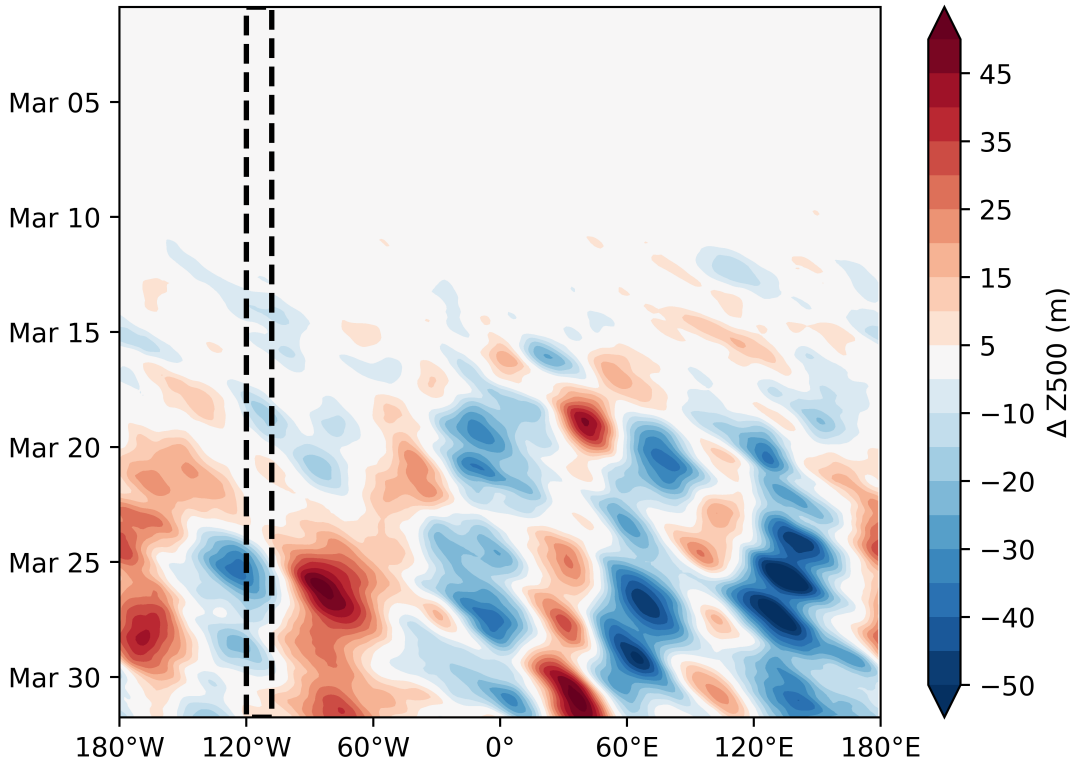

Fig. 11. Hovmöller diagram of March 3-hourly changes in Z500 following Southwest US (outlined) soil moisture depletion on March 1st, averaged from 40º-60ºN over 50 ensemble members.

Figure 11 presents the time evolution of the 500 mb geopotential height anomalies averaged between 40º-60ºN during the first month of the experiment as a Hovmöller diagram. Two weeks after the instantaneous depletion of surface soil moisture on March 1st, a nearly stationary wavenumber 4 Rossby wave sets in with a low center over the western US (~130ºW-90ºW); it takes a little over two weeks for the large-scale pattern to set up and become quasi-stationary, which is consistent with the two-week timescale Teng et al. (2019) found in their study.

Previous work by Branstator (1990, 2002) provides a framework for understanding how local heating sources can excite quasi-stationary wave anomalies within a linear barotropic vorticity model. Recent studies from Koster et al. (2016) and Teng et al. (2019) demonstrated that sensible heating over dry CONUS surfaces produces positive diabatic heating anomalies that are capable of instigating these circulation patterns. However, those studies focused on the contemporaneous circulation response to extended (i.e., 1-3 month) summertime soil moisture deficits prescribed over the Great Plains region and entire Western US domain. To explain the circulation response to a springtime soil moisture deficit in the Southwest US that

we find in our experiment, we examine the evolution of the overlying atmosphere during the first month of the experiment.

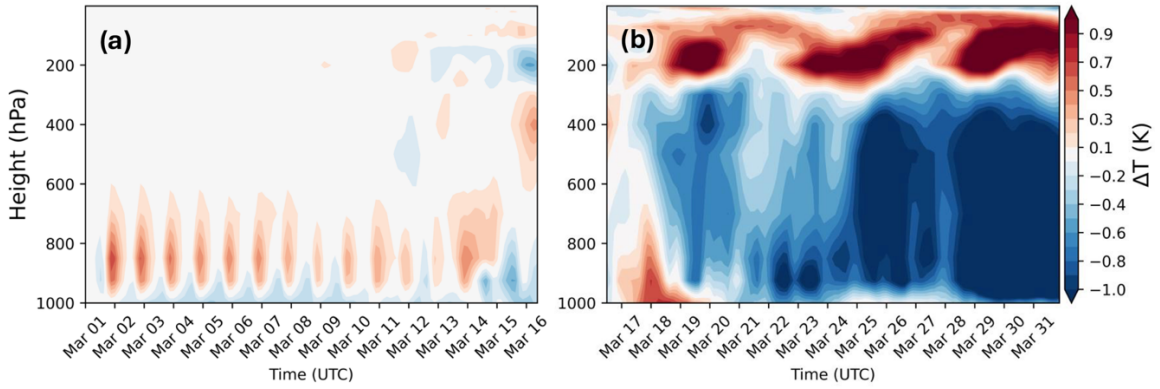

Fig. 12. Vertical changes in March 3-hrly temperature during (a) the first half and (b) the second half of the month following Southwest US soil moisture depletion on March 1st, averaged over the Southwest US depletion region for 50 ensemble members.

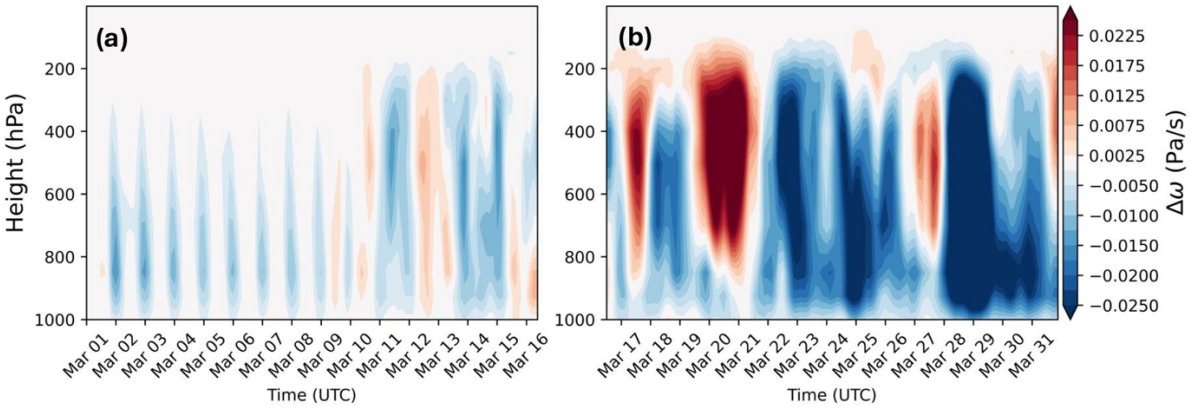

Fig. 13. Vertical changes in March 3-hrly vertical velocity (omega) in pressure coordinates during (a) the first half and (b) the second half of the month following Southwest US soil moisture depletion on March 1st, averaged over the Southwest US depletion region for 50 ensemble members.

Earlier in Section 3, we noted that the Southwest US experienced near-surface averaged cooling in the March monthly mean of our experiments (Fig. 3a). When we examine the composite time series of March air temperature anomalies averaged over the Southwest US, however, we find anomalously warm and rising air in the daytime that extends throughout the troposphere during the first half of the month (Figs. 12a, 13a). In the two weeks immediately following surface soil moisture depletion, temperatures warm by approximately 0.2-0.6ºC from the surface up to 600 hPa, with the strongest warming occurring near the surface during the daytime (Fig. 12a). The negative ω anomalies extend upwards to about 400 hPa (Fig 13a.). At around the two-week mark, the overlying atmosphere gradually becomes dominated by the deep, larger scale motions driven by the circulation response (c.f. Fig. 11)—which,

again, is consistent with the timescales displayed in previous studies. The negative temperature anomalies in the second half of the month (Fig. 12b) are associated with upward vertical motion ($\omega < 0$; Fig. 13b), which is indicative of adiabatic cooling of the troposphere over the Southwest US. We hypothesize that the stretching associated with daytime warming in the first half of the month provides a vorticity source that is responsible for large-scale circulation anomalies in the second half of the month, and that the large-scale circulation response is shaped by the climatological waveguide.

6. The amplitude of the simulated response compared to observations

The a priori assumptions in our study are primarily based upon our knowledge of the WUS-STP from observations (Vargas Zeppetello et al. 2024). While it is difficult to make direct comparisons between the results of our instantaneous forcing and the real-world MAM soil moisture deficits associated with the WUS-STP, we find strong evidence that the teleconnections and processes acting to produce early summer temperature anomalies in our experiment are also relevant to producing the pattern of observed summertime temperature anomalies in the Western US.

To evaluate the amplitude of the simulated response against observations, we first create an index of MAM soil moisture in the Southwest US by averaging detrended satellite measurements of soil moisture over the depletion region in our experiments (see Methods). Following Koster et al. (2016), we then standardize the soil moisture anomalies before regressing them upon observations of summertime temperature and circulation. Vargas Zeppetello et al. (2024) demonstrated that MAM soil moisture anomalies in the Western US are well-correlated throughout the soil column, down to a depth of 50 cm; in our depletion experiments, we find that climatological MAM 50 cm soil moisture is reduced by ~1.2σ on average over the Southwest US. To be consistent in our comparison between observed and simulated amplitudes, we scale the observed response to reflect a 1.2σ reduction in Southwest US MAM 50 cm soil moisture.

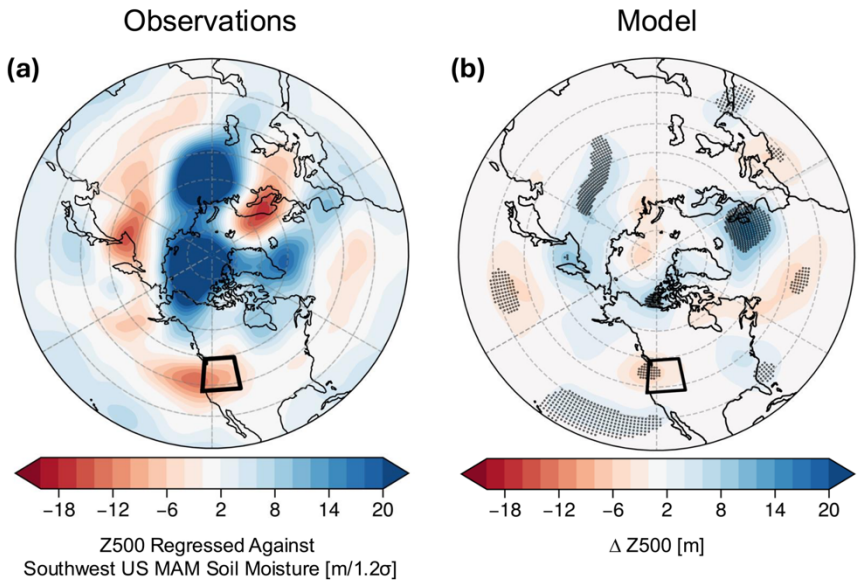

Fig. 14. (a) High pass-filtered MAM average soil moisture across the Southwest US depletion domain from ESA CCI regressed upon May-June 500 mb geopotential heights (Z500) from ERA5. (b) The May-June Z500 change in our depleted soil moisture experiments. Anomalies in (a) are scaled to match the 1.2σ reduction in 50 cm Southwest US MAM soil moisture generated by our experiment.

When we regress May-June 500 mb heights (Z500) from ERA5 against our standardized soil moisture index, we observe (scaled) circulation anomalies are stronger than the simulated response. In observations, a 1.2σ reduction in Southwest US MAM soil moisture is associated with a distal (i.e., non-local) May-June 500 mb geopotential height anomaly of +8.0 m, averaged over the Western US (Fig. 14a, outlined domain). In contrast, Z500 only increases by an average of 3.2 m over the Western US in May-June of our experiments (Fig. 14b). This suggests that the amplitude of the simulated circulation response may be too weak in the model—despite it reproducing the position of the WUS high pressure anomaly. Similarly, Koster et al. (2016) also reported that the circulation response to prescribed soil moisture anomalies was weaker in their model than in nature.

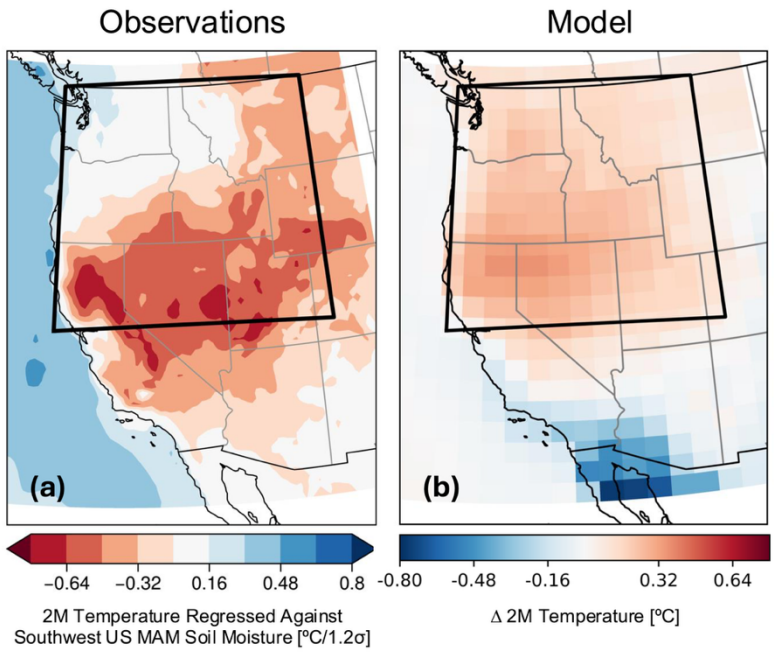

Fig. 15. (a) High pass-filtered MAM average soil moisture across the Southwest US depletion domain from ESA CCI regressed upon May-June 2-m air temperature from ERA5. (b) The May-June 2-m air temperature change in our depleted soil moisture experiments. Anomalies in (a) are scaled to match the 1.2σ reduction in 50 cm Southwest US MAM soil moisture generated by our experiment.

Finally, we compare the amplitude of the simulated temperature response to observations by regressing May-June temperature from ERA5 upon the MAM soil moisture index. From Figure 15a, we expect May-June temperatures to warm by an average of 0.31ºC over the Western US (outlined) in response to a 1.2σ reduction in Southwest US MAM soil moisture in observations. Our experiments, however, only simulate ~61% of the observed temperature response (0.19ºC; Fig. 15b).

Given our hypothesis that circulation changes drive May-June warming in our experiments, that a weak circulation response would also lead to weak temperature anomalies is consistent with our understanding of the processes that modulate summertime temperature variability over the Western US. We note that the relationship between Western US summertime warming and springtime soil moisture anomalies in the five other CMIP6 models analyzed by Vargas Zeppetello et al. (2024) was also considerably weaker than in observations. While identifying model processes leading to this bias is beyond the scope of this paper, we hypothesize that the weak amplitudes of the circulation and temperature anomalies in early summer are related to the weaker persistence in the simulated response compared to that in observations.

7. Conclusion

In this study, we explored the potential for regional springtime soil moisture variations to produce distal teleconnections in summertime temperature and precipitation through land-atmosphere interactions. Building from observations that connect anomalously warm and dry conditions in summer in the Western US to deficits in springtime soil moisture in the Southwest US, we performed an ensemble of experiments using the CESM2 and set the near-surface soil moisture in the Southwest US to zero on May 1st each year. As a result, we found:

I. In March: Reductions in surface latent heat flux over the Southwest US persist to drive daytime diabatic heating anomalies that extend into the upper troposphere during the first half of the month, exciting a large-scale (circumglobal) quasi-stationary wave response.

II. From late March-May: The circumglobal circulation response gives rise to large-scale deficits in precipitation, near-surface relative humidity, and cloudiness over the Western United States.

III. In May-June: Decreases in low-cloud fraction promote widespread warming that begins in the Pacific Northwest through the shortwave cloud radiative effect. Warming is accompanied by Northwest US surface soil moisture deficits that persist into late summer.

In summary, we have demonstrated a new pathway for springtime soil moisture anomalies to have a non-local impact on summertime climate in the Western US. Our results are generally consistent with the observed relationships between springtime soil moisture variations in the Southwest US and summertime temperature and circulation anomalies across the Western US (Vargas Zeppetello et al., 2024). However, the amplitudes of the simulated temperature and circulation responses in early summer are weaker than observed variations associated with a comparable reduction in Southwest US MAM soil moisture, which may also negatively impact persistence.

Though the results of our experiments demonstrate that soil moisture deficits over the Southwest US in March *cause* May-June warming across the Western US, there are a few aspects of the proposed pathway that merit further investigation. First, we would like to investigate the relationship between the amplitude and persistence of the summertime temperature and circulation anomalies to the depth, magnitude, and sign of the initial soil moisture anomaly imposed in springtime. Results from sensitivity studies performed by Teng

et al. (2019) whereby soil moisture anomalies of various amplitudes and depths were imposed throughout the summer suggest that the pattern of circulation anomalies simulated in our experiments will be relatively insensitive to these details, but that the amplitude of the response would scale linearly with the strength of the soil moisture anomaly. Second, we would like to better understand how the atmospheric circulation anomalies in April in response to March soil moisture deficits evolve to produce the pattern of highs and lows in May. Finally, we would like to test whether other climate models reproduce our results in CESM2. Given that the five other CMIP6 models analyzed by Vargas Zeppetello et al. (2024) displayed similar relationships between springtime soil moisture and summertime temperature in their free-running simulations, there is reason to expect consistent representation of the WUS-STP and the physical processes that drive it across climate models.

The presence of soil moisture teleconnections in the Western US extends our understanding of the spatial and temporal scales of land-atmosphere interactions. Our finding that springtime soil moisture deficit in the Southwest US leads to summertime warming and drying across the Western US can potentially be used to improve seasonal forecasts for the region and, more broadly, highlights the need for accurate land initialization schemes within operational models. Moving forward, we are interested in using our methodology to identify similar, teleconnection-like patterns in other regions where antecedent soil moisture conditions may have non-local impacts on climate.

Acknowledgments.

The authors thank Abby Swann and Cecilia Bitz for providing their CESM2 expertise and other scientific insights. LNZ is supported by the National Science Foundation Graduate Research Fellowship under Grant No. DGE-2140004. DSB was supported by a grant from the Tamaki Foundation. High-performance computing support from the Derecho system (doi:10.5065/qx9a-pg09) was provided by the NSF National Center for Atmospheric Research (NCAR), sponsored by the National Science Foundation.

Data Availability Statement.

All observational datasets used in this study are publicly available. The numerical model simulations upon which this study is based are too large to archive. Instead, we provide detailed instructions for replicating the simulations in Section 2, Methods. The model version used was CESM2.1.5.

REFERENCES

Ångström, A., 1935: Teleconnections of Climatic Changes in Present Time. *Geogr. Ann.*, **17**, 242–258, https://doi.org/10.2307/519964.

Berg, A., B. Lintner, K. Findell, and A. Giannini, 2017: Soil Moisture Influence on Seasonality and Large-Scale Circulation in Simulations of the West African Monsoon, https://doi.org/10.1175/JCLI-D-15-0877.1.

Branstator, G., 1990: Low-Frequency Patterns Induced by Stationary Waves.

——, 2002: Circumglobal Teleconnections, the Jet Stream Waveguide, and the North Atlantic Oscillation.

Computational and Information Systems Laboratory. 2023. Derecho: HPE Cray EX System (University Community Computing). Boulder, CO: NSF National Center for Atmospheric Research. doi:10.5065/qx9a-pg09.

Danabasoglu, G., and Coauthors, 2020: The Community Earth System Model Version 2 (CESM2). *J. Adv. Model. Earth Syst.*, **12**, e2019MS001916, https://doi.org/10.1029/2019MS001916.

Delworth, T., and S. Manabe, 1989: The Influence of Soil Wetness on Near-Surface Atmospheric Variability.

Dirmeyer, P. A., 2000: Using a Global Soil Wetness Dataset to Improve Seasonal Climate Simulation. *J. Clim.*, **13**, 2900–2922, https://doi.org/10.1175/1520-0442(2000)013<2900:UAGSWD>2.0.CO;2.

Dorigo, W., and Coauthors, 2017: ESA CCI Soil Moisture for improved Earth system understanding: State-of-the art and future directions. *Remote Sens. Environ.*, **203**, 185–215, https://doi.org/10.1016/j.rse.2017.07.001.

——, and Coauthors, 2021: The International Soil Moisture Network: Serving Earth system science for over a decade. Hydrol. Earth Syst. Sci., 25, 5749–5804, https://doi.org/10.5194/ hess-25-5749-2021.

Douville, H., 2002: Influence of Soil Moisture on the Asian and African Monsoons. Part II: Interannual Variability.

Fennessy, M. J., and J. Shukla, 1999: Impact of Initial Soil Wetness on Seasonal Atmospheric Prediction.

Fischer, E. M., S. I. Seneviratne, P. L. Vidale, D. Lüthi, and C. Schär, 2007: Soil Moisture–Atmosphere Interactions during the 2003 European Summer Heat Wave, https://doi.org/10.1175/JCLI4288.1.

Guo, Z., P. A. Dirmeyer, and T. DelSole, 2011: Land surface impacts on subseasonal and seasonal predictability. *Geophys. Res. Lett.*, **38**, https://doi.org/10.1029/2011GL049945.

Harris, I., T. J. Osborn, P. Jones, and D. Lister, 2020: Version 4 of the CRU TS monthly high-resolution gridded multivariate climate dataset. Sci. Data, 7, 109, https://doi.org/10.1038/s41597020-0453-3.

Hersbach, H., B. Bell, P. Berrisford, and A. Horányi,: ERA5 monthly averaged data on single levels from 1940 to present, accessed 17 July 2025, https://doi.org/10.24381/cds.f17050d7.

Koster, R. D., and Coauthors, 2010: Contribution of land surface initialization to subseasonal forecast skill: First results from a multi-model experiment. *Geophys. Res. Lett.*, **37**, https://doi.org/10.1029/2009GL041677.

——, and Coauthors, 2011: The Second Phase of the Global Land–Atmosphere Coupling Experiment: Soil Moisture Contributions to Subseasonal Forecast Skill, https://doi.org/10.1175/2011JHM1365.1.

Koster, R. D., Y. Chang, H. Wang, and S. D. Schubert, 2016: Impacts of Local Soil Moisture Anomalies on the Atmospheric Circulation and on Remote Surface Meteorological Fields during Boreal Summer: A Comprehensive Analysis over North America. *J. Clim.*, **29**, 7345–7364, https://doi.org/10.1175/JCLI-D-16-0192.1.

Lawrence, D. M., and Coauthors, 2019: The Community Land Model Version 5: Description of New Features, Benchmarking, and Impact of Forcing Uncertainty. *J. Adv. Model. Earth Syst.*, **11**, 4245–4287, https://doi.org/10.1029/2018MS001583.

Liu, D., G. Wang, R. Mei, Z. Yu, and M. Yu, 2014: Impact of initial soil moisture anomalies on climate mean and extremes over Asia. *J. Geophys. Res. Atmospheres*, **119**, 529–545, https://doi.org/10.1002/2013JD020890.

Liu, T., and Coauthors, 2023: Teleconnections among tipping elements in the Earth system. *Nat. Clim. Change*, **13**, 67–74, https://doi.org/10.1038/s41558-022-01558-4.

Lorenz, R., E. B. Jaeger, and S. I. Seneviratne, 2010: Persistence of heat waves and its link to soil moisture memory. *Geophys. Res. Lett.*, **37**, https://doi.org/10.1029/2010GL042764.

McColl, K. A., S. H. Alemohammad, R. Akbar, A. G. Konings, S. Yueh, and D. Entekhabi, 2017: The global distribution and dynamics of surface soil moisture. *Nat. Geosci.*, **10**, 100–104, https://doi.org/10.1038/ngeo2868.

Pal, J. S., and E. A. B. Eltahir, 2001: Pathways Relating Soil Moisture Conditions to Future Summer Rainfall within a Model of the Land–Atmosphere System.

Paolino, D. A., J. L. Kinter, B. P. Kirtman, D. Min, and D. M. Straus, 2012: The Impact of Land Surface and Atmospheric Initialization on Seasonal Forecasts with CCSM, https://doi.org/10.1175/2011JCLI3934.1.

Pincus, R., P. A. Hubanks, S. Platnick, K. Meyer, R. E. Holz, D. Botambekov, and C. J. Wall, 2023: Updated observations of clouds by MODIS for global model assessment. *Earth Syst. Sci. Data*, **15**, 2483–2497, https://doi.org/10.5194/essd-15-2483-2023.

Rahman, M. M., M. Lu, and K. H. Kyi, 2015: Variability of soil moisture memory for wet and dry basins. *J. Hydrol.*, **523**, 107–118, https://doi.org/10.1016/j.jhydrol.2015.01.033.

Rahmati, M., and Coauthors, 2024: Soil Moisture Memory: State-Of-The-Art and the Way Forward. *Rev. Geophys.*, **62**, e2023RG000828, https://doi.org/10.1029/2023RG000828.

Rai, A., S. K. Saha, S. Pokhrel, K. Sujith, and S. Halder, 2015: Influence of preonset land atmospheric conditions on the Indian summer monsoon rainfall variability. *J. Geophys. Res. Atmospheres*, **120**, 4551–4563, https://doi.org/10.1002/2015JD023159.

539 Rohde, R., and Coauthors, 2013: A new estimate of the average earth surface land
540 temperature spanning 1753 to 2011. Geoinfor. Geostat., 1, 1, http://doi.org/10.4172/2327-
541 4581.1000101.

542 Ropelewski, C. F., and M. S. Halpert, 1987: Global and Regional Scale Precipitation
543 Patterns Associated with the El Niño/Southern Oscillation.

544 Schär, C., D. Lüthi, U. Beyerle, and E. Heise, 1999: The Soil–Precipitation Feedback: A
545 Process Study with a Regional Climate Model.

546 Seneviratne, S. I., T. Corti, E. L. Davin, M. Hirschi, E. B. Jaeger, I. Lehner, B. Orlowsky,
547 and A. J. Teuling, 2010: Investigating soil moisture–climate interactions in a changing
548 climate: A review. *Earth-Sci. Rev.*, **99**, 125–161,
549 https://doi.org/10.1016/j.earscirev.2010.02.004.

550 Shukla, J., and Y. Mintz, 1982: Influence of Land-Surface Evapotranspiration on the
551 Earth's Climate. *Science*, **215**, 1498–1501, https://doi.org/10.1126/science.215.4539.1498.

552 Small, E. E., 2001: The influence of soil moisture anomalies on variability of the North
553 American Monsoon System. *Geophys. Res. Lett.*, **28**, 139–142,
554 https://doi.org/10.1029/2000GL011652.

555 Teng, H., G. Branstator, A. B. Tawfik, and P. Callaghan, 2019: Circumglobal Response
556 to Prescribed Soil Moisture over North America. *J. Clim.*, **32**, 4525–4545,
557 https://doi.org/10.1175/JCLI-D-18-0823.1.

558 Trenberth, K. E., G. W. Branstator, D. Karoly, A. Kumar, N.-C. Lau, and C. Ropelewski,
559 1998: Progress during TOGA in understanding and modeling global teleconnections
560 associated with tropical sea surface temperatures. *J. Geophys. Res. Oceans*, **103**, 14291–
561 14324, https://doi.org/10.1029/97JC01444.

562 Ullah, W., W. Guojie, Z. Gao, D. F. T. Hagan, A. S. Bhatti, and C. Zhua, 2021: Observed
563 Linkage between Tibetan Plateau Soil Moisture and South Asian Summer Precipitation and
564 the Possible Mechanism, https://doi.org/10.1175/JCLI-D-20-0347.1.

565 Vargas Zeppetello, L. R., D. S. Battisti, and M. B. Baker, 2022: The Physics of Heat
566 Waves: What Causes Extremely High Summertime Temperatures?,
567 https://doi.org/10.1175/JCLI-D-21-0236.1.

——, L. N. Zhang, D. S. Battisti, and M. M. Laguë, 2024: How Much Does Land–Atmosphere Coupling Influence Summertime Temperature Variability in the Western United States?, https://doi.org/10.1175/JCLI-D-23-0716.1.

Walker, G. T., and E. W. Bliss, 1932: World Weather V. *Mem. R. Meteorol. Soc.*, **4**, 53–84.

Wu, W., and R. E. Dickinson, 2004: Time Scales of Layered Soil Moisture Memory in the Context ofLand–Atmosphere Interaction.

Xue, Y., and Coauthors, 2022: Spring Land Temperature in Tibetan Plateau and Global-Scale Summer Precipitation: Initialization and Improved Prediction, https://doi.org/10.1175/BAMS-D-21-0270.1.

Zhou, S., and Coauthors, 2019: Land–atmosphere feedbacks exacerbate concurrent soil drought and atmospheric aridity. *Proc. Natl. Acad. Sci.*, **116**, 18848–18853, https://doi.org/10.1073/pnas.1904955116.